EAI Endorsed Transactions
on Energy Web
Research Article EAI.EU

Multidimensional Uncertainty Integration based on Spatiotemporal Hybrid Copula: A Resilience-Oriented Modeling Paradigm for IES and Virtual Power Plant

Junxiong Ge[1 *], Lijun Liu[2a], Zhaojun Wang[2b], Xiao Li[2c], Hongxia Guo[2d] and Haimin Hong[1e]

[1]Shenzhen China Gridcom Technology Communication Co., Ltd., 518028, Shenzhen, China
[2]State Grid Shandong Electric Power Company Marketing Service Center, 250002, Shandong, China

Abstract

Integrated Energy Systems (IES) and Virtual Power Plants (VPPs) are pivotal for achieving the "dual-carbon" goals, yet they face significant challenges from multidimensional spatiotemporal uncertainties. Traditional uncertainty modeling methods, relying on static correlation assumptions, are inadequate for dynamically capturing the complex fluctuations in source-load-market parameters, especially the aggregation uncertainties inherent in VPPs. This paper proposes a novel resilience-oriented modeling paradigm centered on a spatiotemporal hybrid Copula (ST-HC) framework. The primary innovation lies in its dynamic correlation capture mechanism, which integrates time-decay and spatial-distance factors to accurately characterize nonlinear, time-varying dependencies among cross-regional uncertainties. Furthermore,a comprehensive five-dimensional evaluation system is established, incorporating metrics for storage flexibility, degradation, market volatility, risk preference, and system efficiency—including a novel data security risk entropy indicator. Validated through case studies, the proposed approach demonstrates superior performance over conventional static models, enhancing planning accuracy and reducing total costs by approximately 9.98%, while effectively quantifying the economic-low-carbon trade-offs under different risk strategies for IES-VPP synergy.

Keywords: IES, Spationtemporal hybrid copula, Dynamic correlations, Multi-dimensional uncertainties

Received on 30 September 2025, accepted on 18 December 2025, published on 15 April 2026

doi: 10.4108/ew.12159

1. Introduction

The transformation of power systems under the "dual-carbon" strategy has drawn significant attention [1,2]. The integration of renewable energy and controllable loads into the grid introduces new challenges for system management, particularly in handling multidimensional uncertainties for IES and VPPs [3-5]. These uncertainties—including fluctuations in renewable generation, randomness of multi-energy loads, volatility of market prices, and data security risks—exhibit complex characteristics such as multi-timescale, nonlinear correlations, and spatiotemporal heterogeneity [6-8]. For VPPs, which aggregate distributed

*Corresponding author: 2125786732@qq.com, [a]18653197662@wo.cn, [b]18254142087@163.com, [c]18615286680@wo.cn, [d]678882088@163.com, [e]honghaimin@sgchip.sgcc.com.cn

resources, additional uncertainties arise from communication reliability and bidding behaviors, further complicating accurate modeling [9].

Traditional uncertainty modeling methods often rely on static correlation assumptions, which fail to capture the dynamic evolution of these interdependencies over time and space [10-12]. This limitation restricts their ability to support the robust planning and operation of integrated IES-VPP systems. While methods like Gaussian Copula and Vine Copula have been applied [13-15,17], they lack mechanisms to adapt to temporal decay and spatial proximity, leading to conservative or inaccurate planning outcomes. Therefore, a method capable of dynamically characterizing spatiotemporal correlations is urgently needed.

To address these challenges, this paper proposes a novel resilience-oriented modeling paradigm for IES and VPPs based on a spatiotemporal hybrid Copula (ST-HC). The main contributions are summarized as follows:

(1) A dynamic spatiotemporal hybrid Copula model is proposed by integrating time-decay factors and spatial-distance weights. This model effectively captures the nonlinear, time-varying correlations among multiple uncertainties, overcoming the limitations of static correlation assumptions.

(2) A unified IES-VPP architectural framework is established, integrating physical energy flows with commercial aggregation mechanisms. This allows for coordinated operation under uncertainty and supports the participation of VPPs in multi-energy markets.

(3) A five-dimensional quantitative evaluation system is developed, incorporating energy storage adjustable margin, degradation rate, power purchase volatility, risk preference, and system conversion efficiency—including data security risk entropy. This system provides a comprehensive metric for assessing the flexibility, risk, and efficiency impacts of uncertainties.

The rest of the paper is organized as follows. Section 2 introduces the IES-VPP architecture and uncertainty sources. Section 3 details the spatiotemporal hybrid Copula modeling framework. Section 4 presents a case study. Finally, Section 5 concludes the paper.

Compared with traditional uncertainty modeling methods based on static correlations or single-dimensional probability distributions, the proposed spatiotemporal hybrid Copula framework exhibits clear advantages in both modeling fidelity and decision support capability. By explicitly incorporating temporal decay and spatial distance factors, the proposed model can dynamically characterize the time-varying and location-dependent dependence structures among source–load–market uncertainties. This enables a more accurate representation of nonlinear coupling effects and avoids excessive conservatism in system planning. Furthermore, the integration of the ST-HC model with a resilience-oriented evaluation system allows the proposed approach to better quantify the trade-off between economic performance and low-carbon objectives under different risk strategies, which is difficult to achieve using conventional static Copula or scenario-based methods.

2. Integrated Energy System Architecture

Figure 1 shows the basic equipment structure of IES, which can be extended to a virtual power plant (VPP) by incorporating distributed energy resources (DERs), communication interfaces, and centralized control systems. In this system, energy inputs are diverse, including fossil fuels, solar, wind energy, and grid power. Among them, the output of renewable energy (such as solar and wind energy) is affected by local climatic conditions, which has significant randomness and uncontrollability, so its input shows strong uncertainty. After the energy is input, it is converted into corresponding energy products (such as electric energy and thermal energy) through various production equipment (such as gas turbines, photovoltaic power generation devices, wind turbines, etc.) in the energy production process, and is collected into energy hubs [18]. Subsequently, the energy is delivered to the end user through transmission networks (e.g. power grids, heat networks, etc.). In a VPP context, distributed resources are aggregated and dispatched as a single entity to participate in market operations, adding a layer of control and uncertainty.

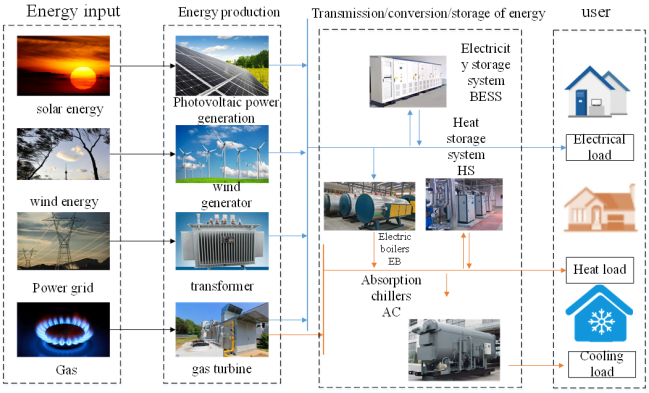

Figure 1. The structural framework of IES

In the energy conversion link, the system realizes the coupling between different energy hubs through a variety of energy conversion devices (such as electric heat converters, cogeneration devices, etc.) to meet the needs of users for multiple energy forms [19-20]. In a VPP, these devices are often distributed and coordinated via a central controller. In addition, the energy storage link can effectively alleviate the imbalance between energy supply and demand in the time dimension and enhance the stability and reliability of the system by configuring different forms of energy storage equipment. Through the collaborative optimization of the above multiple links, the integrated energy system and virtual power plant can achieve efficient use of energy and low-carbon operation, providing important support for the sustainable development of the energy system.

3. Energy Production State

3.1. Energy production

IES's renewable energy units mainly consider solar photovoltaic and wind turbines. The output power of photovoltaics depends on the intensity of solar irradiation, and its energy conversion model is:

$$EP_{pv}^{t} = C_{pv} \cdot f_{pv} \cdot (SI_{pv}^{t} / SI_{pv}^{ra}) \cdot (1 + tc \cdot (T_{pv}^{t} - T_{pv}^{ra})) \quad (1)$$

where, C_{pv} is the installed PV capacity (kW); SI_{pv}^{ra} is therated solar irradiance intensity (W/m²); f_{pv} is the power reduction factor;tc is the temperature coefficient (typically0.004-0.006/°C); T_{pv}^{t} is the temperature of the PV panel surface at time ; T_{pv}^{ra} is the PV panel surface temperature under rated test conditions (°C).

The output power of wind turbines is non-linearly correlated with wind speed, and the energy conversion modelis as follows:

$$P_{wt}^{t} = \begin{cases} 0, v^{t} \le v^{min} \; or \; v^{t} \ge v^{min} \\ \dfrac{\left(v^{t}\right)^{2} - \left(v^{min}\right)^{2}}{\left(v^{ra}\right)^{2} - \left(v^{min}\right)^{2}} C_{wt}, v^{min} \le v^{t} \le v^{ra} \\ C_{wt}, v^{ra} \le v^{t} \le v^{\max} \end{cases} \quad (2)$$

where, $v^{\min}, v^{\max}$ and v^{ra} are cut in, cut out and rated wind speed; C_{wt} is the installed capacity of the wind turbine.

3.2. Energy conversion

The gas turbine realizes the synergistic conversion of chemical energy into heat energy and electrical energy through the combustion process, and its energy conversion model is as follows:

$$EP_{chp}^{t} = \begin{cases} \eta_{chp}^{e,t} \cdot F_{chp}^{t} \cdot LHV_{ng}, & LR_{chp}^{\min} \le LR_{chp}^{t} \le 1 \\ 0, & 0 \le LR_{chp}^{t} < LR_{chp}^{\min} \end{cases}$$
$$HP_{chp}^{t} = \begin{cases} \eta_{chp}^{h,t} \cdot F_{chp}^{t} \cdot LHV_{ng}, & LR_{chp}^{\min} \le LR_{chp}^{t} \le 1 \\ 0, & 0 \le LR_{chp}^{t} < LR_{chp}^{\min} \end{cases} \quad (3)$$

where, EP and HP are electrical power and thermal power (kW/MW); LR is the load factor; F represents the flow rate of natural gas (m^3 /s); η for energy conversion efficiency; LHV has a low calorific value (kJ/ m^3); LR_{chp}^{t} is the load factor of the gas turbine unit at time t; LR_{chp}^{min} is the minimum load factor for the gas turbine unit; LHV_{ng} is the low calorific value of natural gas (kJ/m3); $\eta_{chp}^{e.t}$ and $\eta_{chp}^{h.t}$ for the electrical and thermal efficiency of gas turbine units.

Electrical-thermal conversion equipment is a device that can convert electrical energy into thermal energy, including typical equipment such as electric boilers and geothermal heat pumps. Electric boilers convert electrical energy into heat energy through electric heating pipes, and their electrical energy conversion efficiency usually does not exceed 1. Although there are differences in the coefficient of performance of different electrical-thermal conversion equipment, their core function is to realize the mutual conversion between electrical energy and thermal energy. Therefore, the specific performance parameters of this type of equipment depend on the structural characteristics and operating conditions of the equipment, and the specific performance depends on the type of equipment and operating conditions. Therefore, the electrical-thermal conversion device model is:

$$HP_{e2h}^{t} = \eta_{e2h}^{t} \cdot EP_{e2h}^{t} \quad (4)$$

where, η_{e2h}^{t} it is the conversion coefficient of the electrical-thermal conversion equipment; , EP_{e2h}^{t} , HP_{e2h}^{t} is the input electrical power and the output thermal power at time .

In practical applications, the operation of electric-to-heat conversion equipment needs to follow the constraints of climbing ability:

$$\begin{aligned} HP_{e2h}^{t} - HP_{e2h}^{t-1} &\le UR_{e2h} \cdot \Delta t \\ HP_{e2h}^{t\text{-}1} - HP_{e2h}^{t} &\le DR_{e2h} \cdot \Delta t \end{aligned} \quad (5)$$

where, UR_{e2h} and DR_{e2h} is the upward and downward ramp-up rate of the electric-heat conversion equipment.

At the same time, the real-time power of electricity-heat energy conversion equipment is limited by the installed capacity and needs to meet the power constraints.

$$0 \le HP_{e2h} \le IC_{e2h} \quad (6)$$

where, IC_{e2h} is the installed capacity of electricity-heat conversion equipment.

3.3. Energy storage

The energy state of the electric energy storage system has a temporal correlation, and the energy storage in the current period is determined by the remaining power, real-time charging rate and discharge power in the previous period, and its mathematical model is as follows:

$$E_{es}^{t} = E_{es}^{t-1} \cdot (1 - \chi) + (P_{es \cdot i}^{t-1} - P_{es \cdot e}^{t-1} / \chi_{es.e}) . \Delta t \quad (7)$$

where, χ is the energy loss coefficient of the electric energy storage system; E_{es}^{t} is the energy state of electric energy storage at

time t; $\chi_{es.e}$ is the energy loss coefficient of the electric energy storage system.

If the overcharge and overdischarge conditions need to be strictly avoided during the operation of the electric energy storage system, the energy state needs to meet the following constraints:

$$ESR_{es}^{\min}.C_{es} \le E_{es}^{t} \le ESR_{es}^{\max}.C_{es} \tag{8}$$

where, $ESR_{es}^{\min}$ and $ESR_{es}^{\max}$ is the maximum and minimum energy storage ratio of power storage equipment; C_{es} for the capacity of the electric energy storage system. In addition, its charge-discharge power cannot exceed the maximum charge-discharge power.

$$\begin{aligned} 0 \le P_{es.i}^{t} \le \delta_{es.i}^{t} \cdot \gamma_{es.i}^{\max} \cdot C_{es} \\ 0 \le P_{es.e}^{t} \le \delta_{es.e}^{t} \cdot \gamma_{es.e}^{\max} \cdot C_{es} \end{aligned} \tag{9}$$

where, $\gamma_{es.i}^{\max}$ and $\gamma_{es.e}^{\max}$ is the ratio of the maximum charging. $\delta_{es.i}^{t}$ and $\delta_{es.ees}^{t}$ discharging power of the power storage equipment to the installed capacity; and the operating state parameters of the electric energy storage system at time t. The frequent charge/discharge cycles of the electric energy storage system will accelerate the structural deterioration of the electrode material, resulting in the degradation of equipment performance, and the charge-discharge conversion process is accompanied by significant energy loss. Therefore, it is forbidden to charge and discharge at the same time in the energy storage device, so as to ensure the one-way energy transmission characteristics of the energy storage device.

$$\delta_{es.i}^{t} + \delta_{es.e}^{t} \le 1 \tag{10}$$

After the completion of a cycle, the energy state of the heat storage equipment needs to be restored to the initial state.

$$E_{h}^{t=0} = v_{h}^{0} \cdot C_{h}, E_{h}^{t=0} = E_{h}^{t=|K|} \tag{11}$$

where, v_{h}^{0} is the ratio of the initial state energy of the power storage equipment to the installed capacity; $|K|$ is the length of the scheduling period, which is equal to 24 if the scheduling period is one day.

The energy state of the current operating cycle of the heat storage equipment is determined by the heat storage, heat release power and energy state of the previous cycle.

$$E_{h}^{t} = E_{h}^{t-1} \cdot (1-\chi) + (P_{h\cdot i}^{t-1} - P_{h\cdot e}^{t-1} / \chi_{h.e}).\Delta t \tag{12}$$

Due to the heat capacity threshold of the heat storage medium, the following constraints need to be met.

$$0 \le E_{h}^{t} \le C_{h} \tag{13}$$

where, C_{h} is the installed capacity of the thermal energy storage system. At the same time, the heat storage power and heat release power are also limited by the maximum heat storage/heat release power.

$$\begin{aligned} 0 \le P_{h.i}^{t} \le \delta_{h.i}^{t} \cdot \gamma_{h.i}^{\max} \cdot C_{h} \\ 0 \le P_{h.e}^{t} \le \delta_{h.e}^{t} \cdot \gamma_{h.e}^{\max} \cdot C_{h} \end{aligned} \tag{14}$$

The heat storage and heat release processes of the heat storage equipment lead to the loss of energy, so the heat storage equipment cannot store and release heat at the same time.

$$\delta_{h.i}^{t} + \delta_{h.e}^{t} \le 1 \tag{15}$$

After the completion of a cycle, the energy state of the heat storage equipment needs to be restored to the initial state.

$$E_{h}^{t=0} = v_{h}^{0} \cdot C_{h}, E_{h}^{t=0} = E_{h}^{t=|K|} \tag{16}$$

3.4. System uncertainty constraints

The constraints of multiple uncertainties in IES and VPPs include equipment operating characteristics, dynamic response boundaries, and multi-energy flow coupling balance. In addition to the operating characteristics and constraints of the above-mentioned devices, it also needs to meet the interaction constraints of the grid transmission constraint and the power/thermal power balance of the source-load side, and the system needs to follow the power balance under multiple time scales as follows. For VPPs, additional constraints related to communication latency and aggregation errors must be considered.

Grid interaction constraints:

For IES, the interaction with the power grid needs to meet the requirements of multi-energy flow dynamic balance and system operation stability, and at the same time, the grid connection of IES has a two-way coupling effect on the load peak and valley regulation of the power grid, so the interaction with the power grid has the following constraints:

$$P_{t}^{G} = \tau_{t}^{b} \cdot P_{g,b}^{t} + \tau_{t}^{s} \cdot P_{g,s}^{t}, \forall t \in T \tag{17}$$

$$0 \le P_{g,b}^{t} \le P_{g,b}^{\max}, \forall t \in T \tag{18}$$

$$0 \le P_{g,s}^{t} \le P_{g,s}^{\max}, \forall t \in T \tag{19}$$

$$\tau_{t}^{b} + \tau_{t}^{s} = 1, \forall t \in T \tag{20}$$

where, $P_{g,s}^{t}$, $P_{g,s}^{\max}$ are the maximum value of the purchase and sale of electricity by the system at all times; τ_{t}^{b}, τ_{t}^{s} are the status parameters of the system purchasing and selling electricity at any time, and their values are 0 or 1, and the system purchasing and selling electricity shall not be carried out at the same time.

Electrical power balance:

$$P_{pv}^{t}+P_{wt}^{t}+P_{chp}^{t}+P_{es,e}^{t}+P_{g,b}^{t}-P_{g,s}^{t}-P_{g,a}^{t}=P_{es,i}^{t}+P_{eb}^{t}+P_{d}^{t},\forall t\in T \quad (21)$$

Thermal power balance:

$$Q_{chp}^{t}+Q_{eb}^{t}+Q_{h,e}^{t}\geq Q_{h,i}^{t}+Q_{d}^{t} \quad (22)$$

where, P_d^t and Q_d^t they are the electrical and thermal demand values of the system.

4. Quantitative Evaluation of Multiple Uncertainties and Correlation Modeling

4.1. Sources of systemic uncertainty

The uncertainty of IES and VPPs is mainly due to the multi-dimensional dynamic characteristics of source-load-market coupling, including renewable generation variability, non-stationary load demand, and market price volatility. These uncertainties propagate across coupled heat – electric networks and significantly affect system planning and operation [2,15,16]. For example, wind power output is bimodal due to seasonal differences, and photovoltaic output is intermittent due to cloud shading. Load uncertainty: The demand for cold, heat and electricity is non-stationary, and the load difference between weekdays and holidays is significant, and it is driven by factors such as user behavior and climate mutation. Market uncertainty: Electricity prices and carbon prices are affected by policy regulation, supply and demand, and mixed energy market games, showing non-Gaussian distribution characteristics. Data security risks: New uncertainties such as data tampering and communication delays are closely related to the process of system digitalization. In VPPs, uncertainties also stem from aggregation errors, forecast inaccuracies, and bid-strategy variability.

4.2. Quantitative evaluation system of multiple uncertainties

The quantitative evaluation not only quantifies the economic indicators, investment planning and scheduling schemes, but also focuses on the impact of uncertainty on the dynamic response margin of multi-energy flow coupling, system risk and comprehensive energy efficiency.

Adjustable margin of energy storage system:

The adjustable margin of the energy storage system is the flexible resource that the energy storage device can provide at a certain time, which is divided into upward and downward adjustable margins, which reflects the ability of the energy storage system to adjust and smooth out the fluctuations caused by uncertainty, and the adjustable margin is as follows:

$$Q_t^{+}=\min\left[\rho_{\max}^{d}\cdot Cap,(SOC_t-SOC_{\min})\cdot Cap\right] \quad (23)$$

$$Q_t^{-}=\min\left[\rho_{\max}^{c}\cdot Cap,(SOC_{\max}-SOC_t)\cdot Cap\right] \quad (24)$$

where, Q_t^+ is the upward adjustment margin for energy storage and Q_t^- is the downward adjustment margin for energy storage. $\rho_{\max}^{d}$ and $\rho_{\max}^{c}$ are the maximum charging and discharging energy ratio of electric/thermal energy storage Cap is the capacity of electric/thermal energy storage system, Soc is the energy state of electric/thermal energy storage.

Energy storage system decay rate:

The dynamic response characteristics of the energy storage system are not only reflected in the power fluctuation of charging and discharging, but also the power fluctuation overrun caused by the coupling effect of multiple time scales, which will significantly affect the stability of the operating state of the energy storage and the degradation rate of equipment life. Considering the thermal inertia and the electricity-based nature of the system, the charge-discharge decay rate of energy storage is as follows:

$$C_t^{bess,c}=-\frac{\left|P_{t+\Delta t}^{bess,c}-P_t^{bess,c}\right|}{\Delta t} \quad (25)$$

$$C_t^{bess,d}=\frac{\left|P_{t+\Delta t}^{bess,d}-P_t^{bess,d}\right|}{\Delta t} \quad (26)$$

where, $C_t^{bess,c}$ is the rate of change of energy storage charging power and $C_t^{bess,d}$ is the rate of change of energy storage discharge power.

The rate of change of system power purchases:

As the key energy interaction mode of the multi-source coupling dynamic response system, the change rate of IES and the power grid has a certain impact on the stability of the power grid, so the change rate of power purchase (R_t) is required to reflect the instantaneous change level of power purchase and the disturbance intensity of uncertainty to the power grid, and the change rate of power purchase is as follows:

$$R_t=\frac{\left|P_{t+\Delta t}^{g}-P_t^{g}\right|}{\Delta t} \quad (27)$$

Risk appetite indicators:

The volatility changes brought by uncertainty to the system will lead to an increase in the risk of system operation, which will have a certain impact on the stability and flexibility of the system. For this kind of risk quantification, the conditional value-at-risk theory measures and analyzes the risk brought by uncertainty to the system, and the risk preference index is shown in the following formula:

$$T_c=\vartheta CVaR_\alpha=\vartheta E\left[f(x,\tau)\,|\,f(x,\tau)>VaR_\alpha\right] \quad (28)$$

where, $f(x,\tau)$ is the risk loss function and the uncertainty parameter; τ is a non-negative coefficient, which represents the level of risk preference, and when the value is 0-0.06, ϑ is the risk preference type, and when the value is greater than 0.1, it is the risk aversion type.

The overall conversion efficiency of the system:

The comprehensive energy conversion efficiency of the system characterizes the ratio of the effective energy output to the total input energy of the system, and is a key performance index to measure the energy utilization level of the system. In the context of the "dual carbon" strategy, improving system energy efficiency has become an important way to promote the transformation of energy structure. There are several ways to evaluate comprehensive energy efficiency, such as energy efficiency indicators, which are achieved by the ratio of output energy to input energy, as shown in the following equation:

$$\eta_e = \frac{E_{out}}{E_{in}} \tag{29}$$

The energy efficiency evaluation of IES needs to consider the difference in energy quality of multi-energy flows and the permeability characteristics of renewable energy. Based on the idea of analysis, the energy quality coefficients of different energy forms of the system are introduced into the calculation process of efficiency, as shown in the following formula:

$$\eta_e = \frac{Ex_{out}}{Ex_{in}} = \frac{\sum_j E_{out,j} \cdot \chi_{e,j}}{\sum_i E_{in,i} \cdot \chi_{e,i}} \tag{30}$$

where, $E_{out,j}$ is the energy value of the output energy type of the system is the jtclass of the system, and $\chi_{e,j}$ is the energy quality coefficient of the output energy type of the system is the j class of the system; Enter the energy value of the energy type for the system category i, and $\chi_{e,i}$ is the energy quality coefficient of the energy type for the system category i.

4.3. Multiple uncertainty modeling based on spatiotemporal hybrid copula

IES faces multi-dimensional uncertainties in the source-load-market, including fluctuations in renewable energy output, randomness in load demand, and market price fluctuations. In addition, data security risks (such as privacy leakage and information tampering) in multi-agent interactions further aggravate the complexity of uncertainty representation. Based on the correlation measure of random variables and the modeling and analysis of correlation by Copula function, this paper provides theoretical support for the dynamic coupling model of CESH and the market trading strategy considering dynamic carbon potential feedback. The specific research steps and framework are shown in Figure 2.

Data security risk: An information entropy model is introduced to quantify the risk of information loss in data transmission, as shown in the following formula:

$$H(X) = -\sum p(x)\log p(x) \tag{31}$$

The higher the entropy value, the lower the data security.

The non-parametric estimation model based on kernel function is used to extract the edge distribution characteristics according to the data samples of uncertainty parameters (energy load, photovoltaic output-solar radiation intensity, wind power output-wind speed). In this method, the dependence of parametric modeling on the prior distribution assumption is broken through, and the asymptotic approximation of the true distribution characteristics of random variables is realized through the data-driven mechanism, and the edge distribution estimation model is constructed as follows:

$$f(x) = \sum_{k=1}^{K} \omega_k \cdot \frac{1}{nh_k} \sum_{i=1}^{n} K\left(\frac{x - X_i}{h_k}\right) \tag{32}$$

where, $K(\bullet)$ is the Gaussian kernel function, h_k is the bandwidth of the k-th core, which is satisfied by the corresponding weight; X_i is the sample data, and n is the sample size. The expectation maximization algorithm is used to synthesize the update, and the goal is to minimize the Integral Mean Square Error (MISE):

$$\mathrm{MISE} = \mathrm{E}\left[\int \left(\hat{f}_h(x) - f(x)\right)^2 dx\right] \tag{33}$$

where, $\hat{f}_h(x)$ is the sum density estimation function with bandwidth h; $f(x)$ is a true probability density function; As the expected value, the integral range covers the entire defined domain.

After obtaining the edge cumulative distribution function of uncertain parameters, the correlation of multiple uncertainties (such as wind and solar output, load, electricity price, and carbon price) in IES has spatiotemporal heterogeneity. The static Copula model cannot capture the dynamic changes, and the spatiotemporal weight factor needs to be introduced. The hybrid Copula model with spatiotemporal coupling is shown below:

$$C(u_1,u_2,u_3,u_4) = \theta_G(t,d)C_G + \theta_t(t,d)C_t + \theta_C(t,d)C_{\mathrm{C}} \tag{34}$$

The weight coefficient is determined by the combination of time decay and spatial distance:

$$\theta_i(t,d) = \alpha \cdot e^{-\beta(t-t_0)} + (1-\alpha)\cdot e^{-\gamma d} \tag{35}$$

where, t_0 is the current time; $\alpha = 0.6$, $\beta = 0.1$, $\gamma = 0.05$ are empirical parameters.

The empirical parameters $\alpha = 0.6$, $\beta = 0.1$, $\gamma = 0.05$ are determined based on sensitivity analysis and the practical characteristics of IES–VPP operation. Parameter α reflects the relative importance of temporal and spatial effects in correlation evolution; a value greater than 0.5 indicates that temporal dynamics dominate the dependence variation of renewable output and market prices. The temporal decay coefficient $\beta = 0.1$ corresponds to the short-term memory property commonly observed in wind–solar generation and electricity price fluctuations, while the spatial attenuation coefficient $\gamma = 0.05$ represents moderate regional coupling strength under inter connected grid conditions. This parameter setting achieves a balance between responsiveness to real-time uncertainty and stability of the joint dependence structure.

Common Copula functions include t-copula, Gaussian-copula, Clayton-copula, Frank-copula, Gumbel-copula, etc., and this paper uses the least squared Euclidean distance between the theoretical Copula function and the empirical Copula function as the goodness-of-fit, and selects the appropriate function type.

By obtaining the parameters of the Copula function and determining the appropriate type of Copula function, a multi-dimensional stochastic coupling joint probability distribution model of load demand, renewable energy output and energy market price can be constructed.

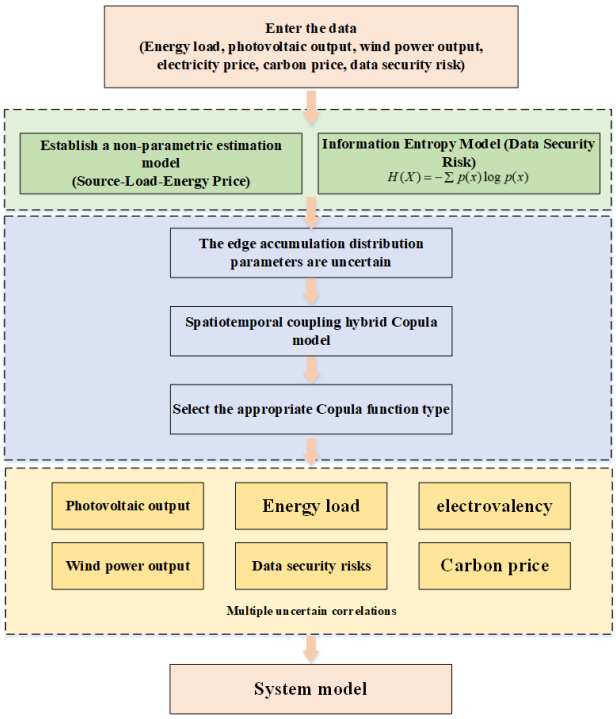

Figure 2. Multi modal uncertainty modeling framework

5. Case Analysis

5.1. Set the parameters of the study

In this paper, a city in northern China is used as an example, and a virtual power plant (VPP) scenario is incorporated to validate the model. The VPP includes distributed PV, wind turbines, and flexible loads. Weather data for a typical meteorological year were obtained from the METEONORM database, and the electricity and heat loads and renewable energy output on typical days in summer, transition season and winter are shown in Figure 3. Based on the load periodicity law, the 24-hour operation cycle is adopted, and the annual operating conditions are characterized by a typical daily scenario set to save the amount of calculation. The energy prices are shown in TABLE 1, and the technical parameters of the main system equipment are shown in TABLE 2.

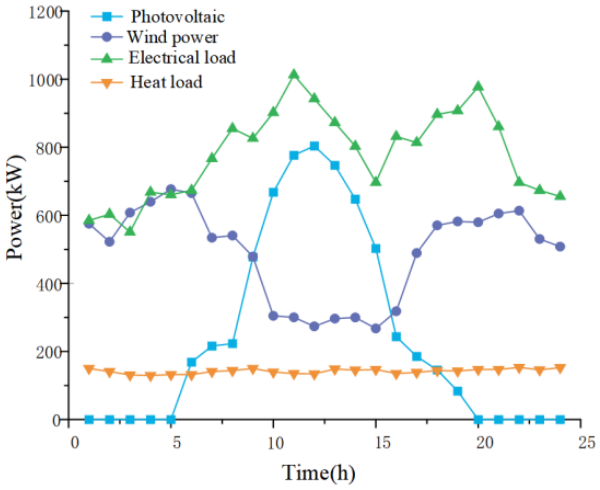

(a) Summer

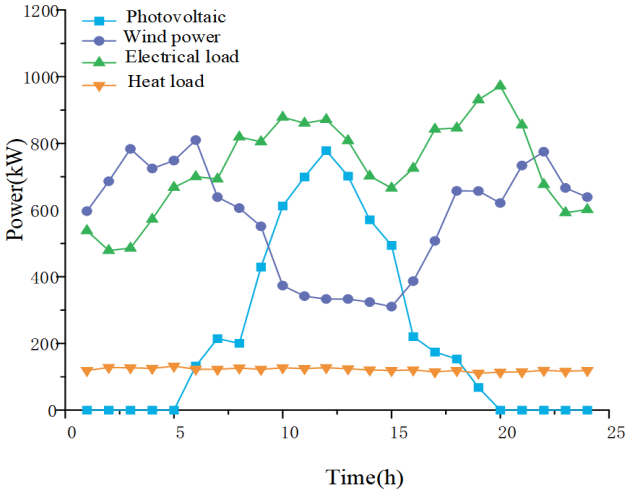

(b)Transation season

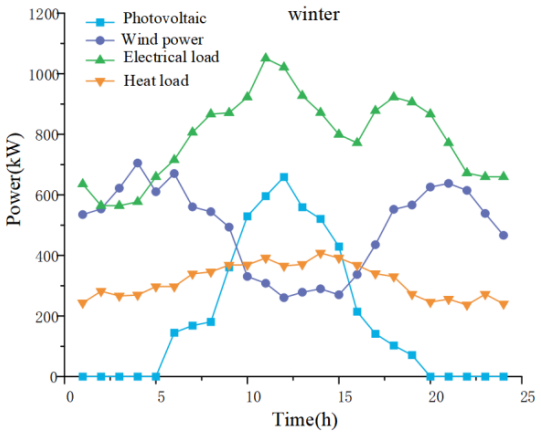

(c) Winter season

Figure 3. Annual typical daily electric heating load and renewable energy output

Table 1. System Energy Prices

Electrovalency	Time	Price
Peak-to-valley electricity prices during non-peak periods	7:00-8:00	0.6259 RMB/kWh
	8:00-11:00	0.9243 RMB/kWh
	11:00-16:00	0.6259 RMB/kWh
	16:00-21:00	0.9243 RMB/kWh
	21:00-23:00	0.6259 RMB/kWh
	23:00-7:00(Next)	0.3275 RMB/kWh
Peak-to-valley electricity prices during peak electricity consumption periods	7:00-8:00	0.6259 RMB/kWh
Electrovalency	Time	Price
Peak-to-valley electricity prices during non-peak periods	8:00-10:00	0.9243 RMB/kWh
	10:00-11:00	1.0462 RMB/kWh
	11:00-16:00	0.6259 RMB/kWh
	16:00-19:00	0.9243 RMB/kWh
	19:00-21:00	1.0462 RMB/kWh
	21:00-23:00	0.6259 RMB/kWh
	23:00-7:00 (Next)	0.3275 RMB/kWh
Natural gas prices	all day	2.4RMB/m^3

Table 2. System Equipment Parameters

parameter	Valid values	parameter	Valid values
gas turbine		Electric boilers	
Dioxide emission factor (kg/m^3)	1.96	Energy conversion efficiency	0.8
Unit maintenance costs (RMB/kWh)	0.05	Maximum output power (kW)	500
Calorific value of natural gas (kWh/m^3)	9.78	Minimum output power (kW)	100
Electricity production efficiency	0.3	Grid interaction	
Heat production efficiency	0.5	CO2 emission factor (kg/kWh)	0.875
Minimum start-stop interval (h)	2	Electricity purchase limits (kW)	250
Minimum output power (kW)	100	Electricity sales limits (kW)	200
Maximum output power (kW)	1000	Carbon tax (RMB/kg)	0.06
Absorption chillers			
Maximum capacity (kWh)	2000		
Cooling efficiency	0.9		
Unit maintenance cost (RMB/kWh)	0.033		

5.2. Multiple uncertainty correlation analysis

In the planning and operation of IES and VPPs, the correlation between multiple uncertainty parameters such as wind power output, photovoltaic output, electricity load, electricity price, carbon price and data risk entropy will affect the system economy and stability. The heat map of IES and VPP multiple uncertainty correlation is shown in Figure 4.

It can be seen from the above figure that there is a weak negative correlation between wind power and photovoltaic output, mainly due to the complementary characteristics of time and space, the peak output of wind power at night and photovoltaic output at noon form a staggered peak, and the wind speed and light under meteorological conditions show a weak negative correlation. There is a strong positive correlation between electricity load and electricity price, reflecting the direct impact of supply and demand imbalance on electricity price fluctuations. There is a strong positive correlation between carbon price and electricity price, which reflects the transmission mechanism of carbon cost to electricity price through energy conversion efficiency and market game, especially under the tiered carbon price mechanism, electricity price fluctuation will amplify the response strength of the carbon market through the carbon

quota elasticity adjustment factor. In addition, the high positive correlation between data risk entropy and electricity price reflects the amplification effect of information coupling risk on market uncertainty, and the data distortion caused by inter-system communication delay will aggravate the error of electricity price prediction, which in turn will affect the system's ability to respond to load fluctuations and renewable energy output intermittently. The strong linkage between electricity priceand load stems from the imbalance between supply and demand. During peak loads, the insufficient reserve capacity of the system leads to a spike in electricity prices, and the data risk entropy increases, indicating that electricity price fluctuations are the core influencing factors of system uncertainty.

Table 3. Parameters of System Energy Storage Equipment

parameter	Valid values	parameter	Valid values
Electric energy storage		Thermal energy storage	
Unit depreciation cost (RMB/kWh)	0.18	Unit maintenance costs (RMB/m^3)	50
Unit installation cost (RMB/kWh)	1020	Unit installation cost (RMB/m^3)	1300
SOC_{max}	0.95	Natural attrition rate	0.05
SOC_{min}	0.2	Thermal storage temperature difference (K)	10
Charging efficiency	0.95	Charging efficiency	0.97
Discharge efficiency	0.95	Exothermic efficiency	0.97
Lifespan (years)	10	Lifespan (years)	25
Maximum charge rate	0.2	Maximum heat rate	0.45
Maximum discharge rate	0.4	Maximum heat release rate	065

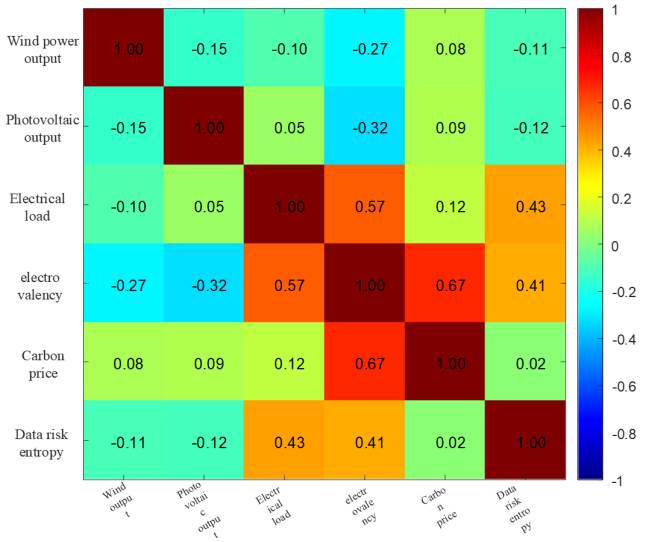

Figure 4. IES multiple uncertainty correlation heatmap

On the one hand, the spatiotemporal complementarity of wind and solar output can reduce the redundancy of system energy storage configuration and stabilize power fluctuations through source-load synergy. On the other hand, the linkage between electricity price and carbon price will exacerbate the entropy increase effect of market risk, and form a dynamic game between economy and low-carbon in extreme scenarios. The dynamic correlation strength of the uncertainty parameters is quantified by the hybrid Copula uncertainty correlation model based on spatiotemporal weight factors, which provides an input constraint boundary for the subsequent system carbon-energy collaboration model, and lays a modeling foundation for the carbon-electricity price elasticity feedback mechanism in multi-agent market transactions considering dynamic carbon potential feedback.

Energy conversion devices (e.g., gas turbines) adhered to ramp-rate limits and power boundaries. Energy storage systems obeyed state-of-charge limits, charge/discharge power constraints, and prohibition of simultaneous charge/discharge Power balance constraints and grid interaction limits were enforced hourly. Failure to satisfy these constraints resulted in solution rejection during stochastic optimization, ensuring feasible system operation under uncertainty.

The collaborative modeling method based on the spatio-temporal hybrid Copula model quantifies the dynamic correlation characteristics of multiple uncertainties of source-load-market. As shown in TABLE 4, compared with the analysis method without multiple uncertain correlations, the thermal energy storage capacity of the system increases by 1.95%, the electric energy storage capacity increases by 3.16%, and the operating cost increases by 8.3%, but the total investment planning cost of the system decreases by 9.98%. Although the increase of system equipment configuration cost lead to the increase of operating cost, the reserve capacity requirement in extreme scenarios is significantly reduced through better uncertainty modeling, and the overall economy of the system and the stability of system operation are ensured.

Table 4. Comparison of system computational complexity under different methods

	Multiple uncertain correlations were not taken into account	Accounting for multiple uncertain correlations
Thermal energy storage capacity (kWh)	257	262
Electric energy storage capacity (kWh)	348	359
Running costs (ten thousand RMB)	58.67	63.54

Total cost (ten thousand RMB)	128.63	115.78

In order to quantify the dynamic correlation characteristics of multiple uncertainties, a spatiotemporal mixed Copula model was constructed, and a composite weight factor composed of a composite weight factor by coupling the time decay factor and the spatial distance factor was used to represent the spatiotemporal heterogeneity of the source-load-market multiple uncertainties. Figure 5 characterizes the influence of spatiotemporal weighting factors on the Copula model.

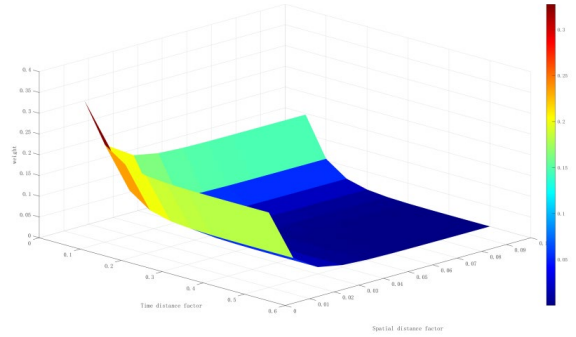

Figure 5. The influence of spatiotemporal weighting factors on Copula model

As can be seen from the above figure 5, the surface shows a significant nonlinear attenuation trend, and the spatiotemporal composite weight factor has a differentiated adjustment mechanism for the Copula model. Specifically, the time decay factor plays a dominant role in the weight: when the time decay factor increases from 0.05 to 0.5, the weight decreases rapidly from 0.82 to 0.36, a decrease of 56.10%. In contrast, when the spatial distance factor increases from 0.01 to 0.1, the weight decreases from 0.75 to 0.43, a decrease of 42.67%, and its weight attenuation contribution is lower than that of the time decay factor.

The time decay factor dominates the weight, which is mainly due to the dynamic correlation between wind and solar output and electricity price fluctuations. For example, PV output is negatively correlated with electricity price, and the decay rate reaches 0.12/h when the time decay factor is 0.12, which effectively characterizes the ability of the time decay factor to capture real-time market transactions. The contribution of the spatial distance factor to the weight attenuation is smaller than that of the time decay factor, which is mainly due to the practical constraints of regional synergy. Among them, the existence of an inflection point indicates that there is a critical state in the model: when the time decay factor is greater than 0.15, the contribution of the time decay factor far exceeds the spatial distance factor. In summary, the spatiotemporal weight factor can effectively quantify the dynamic correlation characteristics of multiple uncertainties through the exponential attenuation mechanism, and provide a modeling basis for the subsequent carbon-electricity price linkage mechanism and market trading strategy.

5.3. Uncertainty analysis that takes into account risk decision

In Figures 6 and 7, considering the impact of multiple uncertainties on the capacity and carbon emissions of each equipment in the system, it can be seen from Figure 6 that the capacity of gas turbines and electric boilers has similar trends. This phenomenon reveals that the system enhances the overall operation stability of the system by improving the installed capacity margin of key equipment in order to absorb the uncertainty disturbance.

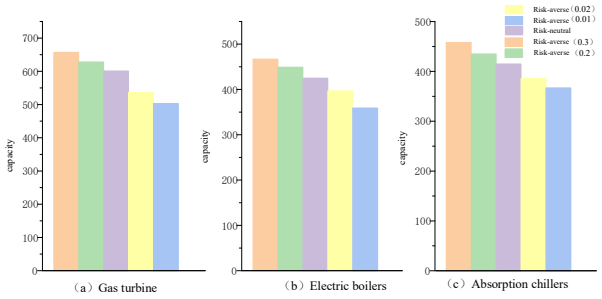

Figure 6. Capacity configuration of system equipment under multiple uncertainties

For the energy storage equipment in the system, the optimal electrical/thermal energy storage capacity configuration of the system shows that the equipment capacity under the risk aversion strategy is significantly higher than that under the risk neutral strategy, and the capacity under the risk neutral strategy is higher than the configuration level under the risk preference mechanism, and the energy storage capacity is positively correlated under the risk aversion mechanism. This indicates that the risk aversion mechanism enhances the risk resistance of the system through the expansion strategy, while the risk appetite mechanism implements capacity optimization according to the principle of economy priority. In summary, the stochastic coupling characteristics of load demand response and renewable energy have a significant impact on the investment planning of multi-energy cogeneration system, and are the key parameters for system investment decision-making and equipment selection.

At the same time, the trend of system carbon emission intensity reveals that the intensification of energy demand volatility will lead to a significant increase in the dependence on fossil energy peak shaving. Under the same risk conditions, the main body of the risk appetite mechanism system tends to optimize the fuel cost structure, reduce the carbon emission intensity by actively reducing the installed capacity allocation of traditional energy, and selectively accept the unplanned risks caused by uncertainty.

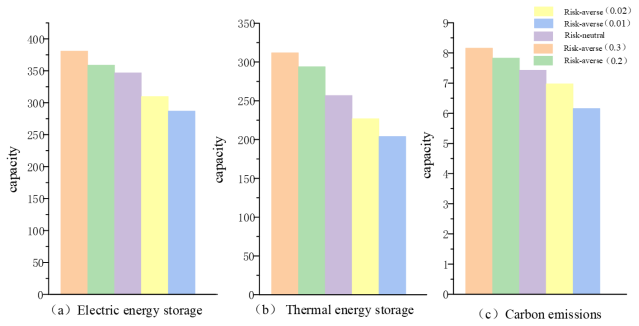

Figure 7. Capacity configuration and carbon emissions of system energy storage equipment under multiple uncertainties

For energy storage adjustable margins (defined in Eq. 23–24), we provide a quantitative example for summer peak hour (15:00) under risk-averse strategy:

Electric storage:

$$\Delta P_{up.e} = \min((0.95-0.75)\times 359, 0.2\times 359) = 71.8\text{kW}$$

$$\Delta P_{down.e} = \min((0.75-0.2)\times 359, 0.4\times 359) = 143.6\text{kW}$$

Thermal storage:

$$\Delta P_{up.h} = \min((0.95-0.70)\times 262, 0.45\times 262) = 65.5\text{kW}$$

$$\Delta P_{down.h} = \min((0.70-0.2)\times 262, 0.65\times 262) = 131.0\text{kW}$$

These margins directly influenced dispatch decisions: During wind power fluctuations, upward marginswere used to absorb excess generation, while downward margins supported load spikes when renewables dropped.

In order to quantify the differential impact of different risk appetites on the planning and operation performance of IES, TABLE 3 compares the impact of risk-averse, risk-neutral and risk-appetite on the system.

The 9.98% reduction in total cost (Table 4) was achieved because the spatiotemporal Copula model accurately captured dynamic correlations, allowing tighter adherence to operational constraints (e.g., avoiding conservative storage SOC limits).

Risk-averse storage capacity increases (Figure 7) directly expanded adjustable margins, enhancing resilience but raising costs (Table 5).

Table 5. Quantitative impact of multimodal uncertainties on system performance under different risk preferences

	Risk-averse	Risk-neutral	Risk-averse
Risk-averse renewable energy consumption rate (%)	45.7	62.5	65.9
Carbon emissions (tCO_2)	1187.6	1267.9	1358.2
Running costs (ten thousand RMB)	62.5	60.4	57.6
Total cost (ten thousand RMB)	126.7	118.4	106.1

Higher operating costs under risk-aversion (62.5 vs. 57.6 kRMB) reflect the cost of maintaining larger storage margins for uncertainty absorption, while lower renewable consumption (45.7% vs. 65.9%) stems from prioritizing dispatchable gas turbines over volatile renewables to ensure constraint compliance.

As can be seen from the above table, the risk-averse type enhances the system's anti-risk ability by increasing the energy storage capacity and gas turbine capacity, but the total cost of equipment redundancy increases by 19.42% compared with the risk-appetite type. On the contrary, the risk appetite strategy reduces the total cost by reducing system equipment investment and flexible load response, but the carbon emission increases by 14.37%. The risk-appetite type has the highest absorption rate, but its operating cost is only 7.84% lower than that of the risk-averse type. This indicates that the high absorption rate of renewable energy is due to the fact that the fluctuation of wind and solar output has not been fully stabilized, and the power gap needs to be filled by gas turbines, which indirectly increases carbon emissions. The risk-neutral strategy achieves a balance between total cost and carbon emissions, and the carbon emissions are reduced by 6.65% compared with the risk-oriented type, indicating that moderate risk appetite can take into account the economics and low-carbon properties of IES. The differential impact of different risk mechanisms on system flexibility resources and market risk transmission is further revealed, which provides support for the subsequent carbon-energy synergy and multi-agent market trading strategies.

It should be noted that dynamic variation in energy storage lifespan degradation may affect the economic–low-carbon trade-off results. Accelerated degradation increases the effective lifecycle cost of storage systems and may reduce their long-term flexibility contribution, leading to a higher reliance on dispatchable fossil-fuel units for balancing under extreme uncertainty scenarios. However, since the proposed framework explicitly incorporates storage degradation indicators into the multi-dimensional evaluation system, the model can adaptively adjust capacity planning and dispatch strategies. Therefore, while degradation dynamics may shift the absolute trade-off boundary, the relative effectiveness of the proposed spatiotemporal Copula-based optimization framework remains robust.

6. Conclusion

This paper proposes a novel resilience-oriented modeling paradigm for Integrated Energy Systems (IES) and Virtual Power Plants (VPPs) based on a spatiotemporal hybrid Copula (ST-HC). The main contributions are threefold:

First, a unified IES-VPP architectural framework is established, integrating multi-energy flows with VPP aggregation logic to enable coordinated operation under a "physical-information-market" perspective. Second, a dynamic ST-HC model is developed, incorporating temporal decay and spatial distance factors to accurately capture nonlinear, time-varying correlations among renewable generation, load, market prices, and data risks—overcoming the limitations of static models. Third, a five-dimensional evaluation system is introduced, combining metrics for storage flexibility, degradation rate, power purchase volatility, risk preference, and system efficiency to holistically assess uncertainty impacts. However, the study also has certain limitations that should be acknowledged. First, although the model has been validated using data from a specific region in China, its performance and parameter sensitivity when applied to different geographical areas with distinct load patterns and market rules require further investigation. Second, the computational complexity of the model, particularly for large-scale systems with numerous uncertainty parameters, may pose challenges for real-time applications or extensive scenario analyses, especially in environments with limited computational resources. Future research will focus on several promising directions. Primarily, efforts will be made to optimize the algorithm's computational efficiency, for instance, by exploring distributed computing frameworks or developing simplified model variants, to enhance its practicality for large-scale, real-time applications. Additionally, exploring the deep integration of this uncertainty modeling framework with actual electricity market bidding strategies and carbon trading mechanisms will be a critical next step. Finally, extending the model's application to interconnected multi-regional IES-VPP clusters and investigating cross-system uncertainty propagation and cooperative optimization represent important avenues for further advancing the security, economy, and sustainability of future energy systems.

References

[1] Smith JA, Müller T, Johnson RW. Spatiotemporal vine copula modeling for correlated uncertainties in multi-energy grids[J]. Applied Energy. 2024; 367: 123301.

[2] Dubois L, Rossi F, Schmidt M. Data-driven nonparametric dependence modeling of wind-solar-load uncertainties using optimal transport copulas[J]. IEEE Transactions on Sustainable Energy. 2023; 14(4): 2101-2115.

[3] Anderson KL, Williams PD. Multimodal uncertainty propagation in renewable-integrated energy hubs: A Gaussian mixture copula approach[J]. Renewable and Sustainable Energy Reviews. 2024; 192: 114201.

[4] Müller S, Braun H, Fischer K. Resilience quantification of IES under spatiotemporally correlated uncertainties using conditional value-at-risk[J]. Energy Economics. 2023; 128: 107261.

[5] García-Sánchez C, Fernández-Guillamón A, Gómez-Lázaro E. Dynamic weighting of temporal-spatial factors in hybrid copula models for energy system uncertainty characterization[J]. Energy Conversion and Management. 2024; 308: 118152.

[6] Patel RK, Jackson ST. Information-theoretic security risk assessment for cyber-physical integrated energy systems[J]. IEEE Transactions on Smart Grid. 2023; 14(5): 4021-4033.

[7] Kazempour J, Pinson P, Papaefthymiou G. Regime-switching copulas for modeling electricity-carbon price dependencies in low-carbon energy planning[J]. Operations Research. 2024; 72(1): 1-19.

[8] Viehweider F, Moser A, Leimgruber F. Exergy efficiency degradation under multi-uncertainty coupling in district energy networks[J]. Energy. 2023; 282: 128742.

[9] Bessa RJ, Matos MA, Costa IC. Multidimensional flexibility metrics for energy storage in correlated uncertainty environments[J]. IEEE Transactions on Power Systems. 2024; 39(1): 511-525.

[10] Hodge BM, Orwig KD, Lew DJ. Copula-entropy frameworks for probabilistic forecasting of multi-energy demand under extreme weather[J]. Renewable Energy. 2023; 218: 119312.

[11] Zima M, Andersson G, Hug G. Adaptive mixed copula models for dynamic correlation analysis of source-load-market uncertainties[J]. Electric Power Systems Research. 2024; 226: 109991.

[12] Smith TJ, Brown MH. CVaR-constrained optimization of integrated energy systems under spatiotemporal uncertainty correlations[J]. International Journal of Electrical Power & Energy Systems. 2023; 152: 109232.

[13] Giannelos S, Konstantelos I, Strbac G. Sparse vine copula constructions for high-dimensional uncertainty modeling in energy systems[J]. Applied Energy. 2024; 355: 122178.

[14] Wogrin S, Tejada-Arango DA, Centeno E. Robust-copula optimization for capacity planning of multi-energy systems under data scarcity[J]. European Journal of Operational Research. 2023; 309(2): 789-803.

[15] Palmintier B, Webster MD. Dynamic correlation risk premiums in electricity-carbon markets: Implications for IES investment[J]. The Energy Journal. 2024; 45(2): 1-28.

[16] Zucker A, Hinz F, Most D. Nonparametric Bayesian networks for uncertainty propagation in integrated heat-electricity networks[J]. Energy. 2023; 274: 127352.

[17] Pinson P, Madsen H, Nielsen HA. Temporal adaptive copulas for short-term forecasting of correlated renewable generation[J]. Wind Energy. 2024; 27(3): 301-317.

[18] Dehghan S, Amjady N, Kazemi A. Resilience-oriented stochastic scheduling of IES under cyber-physical contingencies using hybrid copula[J]. IEEE Transactions on Industrial Informatics. 2023; 19(7): 8201-8212.

[19] Zugno M, Morales JM, Pinson P. Equilibrium models for electricity markets with correlated wind and price uncertainties[J]. Mathematical Programming. 2024; 201(1-2): 1-32.

[20] Bottieau J, De Grève Z, Vallee F. Multiscale copula-based scenario generation for coordinated energy storage dispatch[J]. Journal of Energy Storage. 2023; 68: 107732.